ASSESSING BIOMASS STEAM GASIFICATION TECHNOLOGIES USING A MULTI-PURPOSE MODEL

Angelo Maria Sepe[1], Jun Li[2], and Manosh C Paul[1*]

[1]Systems, Power & Energy Research Division, School of Engineering, University of Glasgow, Glasgow G12 8QQ, UK

[2]Chemical & Process Engineering Department, University of Strathclyde, Glasgow G1 1XJ, UK

*Corresponding author: Manosh.Paul@glasgow.ac.uk, +44 (0)141 330 8466

Abstract

Two advanced steam-gasification technologies of biomass, high temperature steam gasification (HTSG) and solar-assisted steam gasification, have been thermodynamically investigated in this work and compared with both conventional auto-thermal gasification and High Temperature Air and Steam Gasification (HTAG). A multi-phase, multi-physics 1D steady-state model has been built up to predict the biomass gasification performance, efficiency, yield and species of produced syngas at varying gasification methods and input parameters. In particular, heterogeneous and homogenous gasification reactions coupled with a radiative transfer were employed in the solar-assisted steam gasification. The results showed that the solar-assisted steam gasification technology demonstrates its potential to produce high quality syngas (nearly 42% H_2 and 35% CO). Moreover, it upgrades the heating value of the product syngas up to 1.4 times more than the original value, due to the additional solar energy induction. Compared with conventional auto-thermal gasification, it was found that the process efficiency can be improved from 65% to 81% if using the HTAG technology and the content of hydrogen in the syngas increased from 30% to 55% if applying HTSG. The modelling results agree considerably with the reported experimental and modelling data in literature, and also able to return a direct comparison of advantage and disadvantage of each gasification method, in terms of syngas quantity and quality.

Keywords: Gasification technology; numerical modelling; biomass; high temperature steam gasification; solar-assisted gasification

1 Introduction

The majority of greenhouse gas emissions are coming from the combustion of fossil fuels, which is still the predominant way of producing energy. One of the most important challenges today is the development of sustainable energy processes to meet the increasing demand of energy that are also able to slash down carbon emissions and carbon footprint. Recently, a renewed interested has arisen in gasification due to new carbon capture storage (CCS) and CO_2 removal technologies, which are based on Integrated Gasification Combined Cycle (IGCC) power plant, where the syngas derived from gasification of coal or biomass is utilised to produce energy.

The gasification process for excellence has always been, and still is, the auto-thermal process, where high temperatures are able to process the characteristic gasification reactions, through a partial combustion of biomass feedstocks. However, this method produces pollutants as outputs (e.g. CO_2 and other impurities) and has relatively low chemical conversion efficiency. The literature on the autothermal gasification is vast, a review of the state of art of the technology can be found in [5] and [6].

Several publications have also appeared in recent years documenting the feasibility of gasification of biomass using an external heating source ('allothermal' gasification) using steam [3] or CO_2 [25, 26] as an agent, where the temperatures necessary to drive the high endothermic gasification reaction can be developed by the gasification agent itself, steam.

Using Steam based technologies, a syngas with high heating value (LHV) and H_2 rich was obtained using various types of reactors [6–8]. For steam only technologies, there are several additional advantages: (1) No combustion derived pollutants; (2) No dilution caused by presence of N_2 in the end gas; (3) No oxygen plant is required respects to an air/oxygen blown gasifier.

The methods to obtain syngas using steam as a gasification agent can be categorised as partial steam or air/steam mix injection and steam-only gasification. The former would be a classic autothermal process with low temperature steam injection or with a high temperature air/steam mixture called High Temperature Agent Gasification (HTAG). The latter comprises two allothermal technologies, i.e. High Temperature Steam Gasification (HTSG) and Solar-driven gasification.

The HTAG represents an alternative method to conventional gasification processes, using both high temperature air and steam as a gasification agent. The rationale of a HTAG is that the preheated gasifying agent at high temperature carries enthalpy that is able to replace the energy required by the partial fuel oxidation in traditional gasification technology. In this way, a larger percentage of feedstocks can be converted into syngas. Several studies indicate that the application of preheated air-steam is able to enhance syngas quality and raise the overall energy efficiency of the process [9,10].

Without air injection and partial combustion, the steam gasification process is more complex, since the heat required to drive gasification reactions is not internally provided by combustion of part of feedstock but by external heat resources. This is realized either by pre-heating the steam before injection into the bed, e.g. High Temperature Steam gasification (HTSG), or heating the solid bed through direct heat flow, e.g. Solar Gasification.

Previous researches have demonstrated HTSG is able to generate a H_2 rich gas, up to 40% vol/vol, using different wood biomass as feedstock in a fixed bed reactor [11,12], in which preheated steam at temperatures up to 1334K was used as a gasification agent. The hydrogen's yield was found to be greatly influenced by the steam/carbon ratio. The steam/carbon ratio needs to be carefully chosen to optimize the ratio of H_2/CO_2 since unwanted CO_2 was found to account to up to 30% in the producer gas.

A promising alternative to the conventional gasification is represented by solar-assisted steam gasification, which can convert biomass feedstocks into a quality syngas, high in H_2 content and low in CO_2. Solar gasification experimental setups using various carbonaceous materials [13,14] showed that carbon dioxide concentration decreased as much as temperature in the solar reactor increased. In the cited studies, CO_2 was found to account for less than 1% at 1600K, while H_2 production was around 40%. Different methods to collect solar power were used to heat packed-bed reactors by means of optical systems. A complete review of the state of arts of solar gasification technology can be found in [6,15].

Two modelling approaches, thermodynamic equilibrium and reaction kinetics, are mostly used in literature to solve the gasification problem. Although the equilibrium model, also known as a 0D model, is vastly used for its simplicity and gives a reasonable grade of result accuracy, it does not show the inner mechanisms of the gasification process. The latter, instead, describes the various stages of the gasification process (drying, pyrolysis, gasification) from the physical-chemical point of view. A set of empirical equations is used in describing both the chemical reactions and heat-mass transfer phenomena in 1-D, 2D or 3D dimensions. An example of 0D model for steam and solar gasification can be found in [14], where it was used to predict the output of a combined drop-tube and fixed-bed reactor. A 1-D model was proposed for an indirectly-irradiated solar reactor consisting of two cavities separated by a radiant emitter, with the upper one serving as the solar radiative absorber and the lower one containing the reacting packed bed [16]. A one-dimensional model based on auto-thermal gasification reactions kinetics has been proposed to simulate and validate an updraft fixed-bed HTSG pilot plant [17]. The plant utilised super-heated steam at a temperature above 1273 K. A successful attempt to create and solve 2-D models is in [18], where an HTAG model was developed to study the gasification process in a downdraft configuration. The gas and solid phases were resolved using Euler−Euler multiphase approach. The model results were compared with experimental data

from a demonstration-scale fixed-bed downdraft gasifier. A solar-driven gasification 2-D model was implemented in [22], where the system consisted of a parabolic and hyperbolic reflector using Cassegrain configuration and advanced CFD tools were used to simulate the system's behaviour.

Despite the recent interests in these new technologies, there is not a vast background of studies and most experimental results are limited to lab scale plants. The numerical models developed in literature, especially for solar gasification, are mostly heavily parametric. Due to the level of sophistication, their use is usually limited to certain pilot plants. Therefore, these models focus more on addressing the experimental plants behaviour than assessing the gasification technologies themselves.

Thus, this paper will present a multi-purpose 1-D numerical model that employs comprehensive reaction kinetics. The model will aim to reasonably predict syngas species and to describe gasification performance of the reactor without focusing on the reactors specific features. The model is able to process various biomasses if the ultimate and proximate data are known. Eventually, the various gasification technologies will be analysed *"vis-à-vis"* obtaining a comprehensive scenario of biomass gasification. The results presented are obtained by simulating the gasification of sugar cane bagasse pellets [19], which are widely used as biomass in other gasification studies ([14,20]), due to its abundance [21], representing a realistic and proper candidate for industrial scale gasification technologies.

The model will be applied to describe the gasification process and its products in a high power packed-bed reactor. The packed or fixed bed configuration was initially proposed for a solar reactor [23], it represents the only common working solution already experimented for all type of gasification technologies. The reactor features will remain fixed for all the simulations to assess the processes' efficiency independently from its design. However, operational parameters will be optimised to offer a comparison of the highest results achievable from each technology regardless of the models limitations.

The solar reactor proposed in this study is supposed to be directly irradiated i.e. the solar input could be provided by a heliostats field. A picture of the proposed solar reactor is shown in Figure 1. The solar flux coming from hyperbolic optics is further concentrated, thanks to a compound parabolic concentrator (CPC) at the top of the cavity receiver. The heating source then passes through a special made quartz window and finally enters into the reactor chamber.

2 Methods

2.1 Model description

In this work a kinetic model is employed to describe the various stages of gasification process (e.g. drying, pyrolysis, combustion, reduction). The model includes reaction kinetics for the fuel drying and devolatization as well as ad hoc kinetics for two-phase flow. This allows to evaluate concentration profiles of all the species that take part in the various reactions and temperature profiles of both solid phase and gas phase along the reactor.

The biomass fed in the reactor is regarded as a mixture of char, volatile matter, water and ash:

$$Biomass \rightarrow Char + volatile + H_2O(l) + Ash$$

The gasifier (Figure 1) has a plain cylindrical shape and a finite volume method (FVM) has been utilised to divide the reactor in a multitude of infinitesimal elements of volume equal to the product of the section of the reactor (A_r) for the height z of the cell. The one dimensional problem formulation for packed-beds is usually sufficiently accurate to describe all the phenomena acting in the reactors without introducing radial derivatives, at least as a first modelling approach [16]. As suggested by several other researchers the bed void section can withstand only minimal variations, in our case, and therefore it is supposed to be constant [24,25].

The power losses in a solar-reactor are principally due to the cavity receiver efficiency, to re-radiation and reflection losses as well as cold-surface radiation losses [16]. In this study heating losses are not considered. The radiation flux inside the reactor will refer then to an after-losses net energy flux.

2.2 Chemistry and kinetics

The first process of gasification undertaken in feedstock is drying where the moisture is removed. Due to the very high temperature reached in the reactor, the drying process $R_{dry} = A_{H_2O} \cdot exp\left(\frac{-E_{H_2O}}{R\,T_s}\right)$ is considered instantaneous and depends only on the solid temperature. A one-step global reaction mechanism is used to represent the chemical process of devolatilization, or pyrolysis, in which volatiles species (CO, CO_2, CH_4, H_2, etc.) and heavy hydrocarbon (e.g. tar) are released from feedstocks. Specifically, it is divided into a primary devolatilization reaction underwent by carbonaceous fuel and a secondary volatile release by tars, usually named tar-cracking:

$$Primary\ pyrolis(Rp1): Biomass \rightarrow aCO + bCO_2 + cCH_4 + dH_2 + eH_2O + ftar + gChar \quad (3)$$

$$Tar\ cracking(Rp2): Tar \rightarrow a1CO + b1CO_2 + c1CH_4 + d1H_2 + e1H_2O \quad (4)$$

with $R_{pyro} = \rho_{biomass} A_{pyro}\, exp\left(\frac{E_{pyro}}{R\,T_s}\right)$ and $R_{tar} = \rho_{tar} A_{tar}\, exp\left(\frac{-E_{tar}}{R\,T_g}\right)$. The biomass devolatilization kinetic was implemented using woody biomass pellets [26]. For a fixed/packed bed reactor the final products yield of this reaction can be considered constant as reported in Table 1. Tar

is modelled as C_6H_8O , as in *Mandl et al.* [27]. Furthermore, in our case, due to the extremely high temperature gradient at the bed entrance and concentrated energy flux, the pyrolysis is considered to be instantaneous (Flash-pyrolysis) [28–30].

The oxidation/combustion reactions contain the following heterogeneous and homogenous reactions.
Heterogeneous reactions:

$$\{Rc_{s1}: C + (1/\varphi)O_2 \rightarrow 2(1-1/\varphi)CO + (2/\varphi - 1)CO_2\ (Oxidation) \tag{5}$$

Homogenous reactions:

$$\begin{cases} Rc_{g1}: CO + ½\, O_2 \rightarrow CO_2\ (Combustion) \\ Rc_{g2}: H_2 + ½\, O_2 \rightarrow H_2O\ (Combustion) \\ Rc_{g3}: CH_4 + 2\, O_2 \rightarrow CO_2 + 2H_2O\ (Combustion) \\ Rc_{tar}: C_mH_n + (m/2 + n/4)\, O_2 \rightarrow mCO_2 + n/2\, H_2O\ (Tar\ oxidation) \end{cases} \tag{6}$$

To model the solid-gas reactions, which can be regarded as char-gas reactions, a shell progressive (SP) or unreacted shrinking core model is implemented. In such mechanism, diffusivity of ash, layer and gas film are taken into account during the reactions. Practically, a stratum of ashes is considered to remain on the particles and wrap the unreacted core. Following that, the external diameter (dp_0) remains unchanged whilst there is a reduction in the inner core d_c. According to [31], without solid experimental data, the SP model seems to be a preferable choice. In addition, a study conducted on carbonaceous fuel particles combustion [32] shows the existence of an ash layer in the packed bed. A set of surface reactions, which comprise both kinetic and diffusion mass transfer rates, can then be formulated as [31,33]:

$$Rs_i = \frac{P_i}{\frac{1}{K_{diff}} + \frac{1}{K_{ash}} \cdot \left(\frac{1}{\xi} - 1\right) + \frac{1}{K_{kin} \cdot \xi^2}} \cdot 6 \cdot \frac{(1-\varepsilon)}{dp_0}$$

with

$$K_{diff,i} = D_i \cdot \left(2.2 \cdot Re^{0.6} {Sc_i}^{1/3}\right) \cdot {d_{p0}}^{-1} \qquad Re = \rho_g \cdot u_g \cdot d_{p0} \cdot {\mu_g}^{-1}$$

$$K_{ash,i} = 2 \cdot D_i \cdot {\varepsilon_{ash}}^{2.5} \cdot {d_{p0}}^{-1} \qquad Sc_i = \mu \frac{\mu_g}{\rho_g \cdot D_i}$$

$$K_{kin,i} = Intrinsic\ reaction\ rate \qquad D_{O_2} = 7.20 \cdot 10^{-4}$$

$$\xi = \frac{d_c}{d_{p0}} = \left(\frac{\rho_{char}}{{\rho^*}_{char}(1-\varepsilon)}\right)^{1/3} \qquad D_{H_2O} = 9.61 \cdot 10^{-4}$$

$$D_{CO_2} = 6.17 \cdot 10^{-4}$$

$$D_{H_2} = 29.02 \cdot 10^{-4}$$

where Rs_i expressed in kg/m^3 s, ε is the ash layer void fraction taken as 0.5, and D_i is the average species diffusivities [34]. $K_{kin,i}$ are the Arrhenius type reaction rates taken from [31], ξ is a parameter that accounts for the char bed density variations along the process and ${\rho^*}_{char}$ is the solid particle density with a diameter equal to d_c . Finally, P_i, component of the partial pressure, is expressed as a

function of the partial density using the ideal gas law. Regarding the combustion factor φ, a value of 2 has been assigned into reaction Rc_{s1}.

The gas-gas kinetics are formulated (Table 2) as a function of the species concentration, $[C_i]$ in kmol/m^3, which are linked to the components partial density and molecular mass by the following relations: $[C_i]=\rho_i/M_i$. For the tar oxidation, the enthalpy of reaction was calculated as $\Delta HRg4 = -393702m - 120971n - \Delta H^0_{298}\, Tar$.

Finally, the steam gasification/reduction chemical process is entirely characterised by the following three surface reactions and two homogenous reactions:

Heterogeneous reactions:
$$\begin{cases} \mathrm{Rs_1: C + CO_2 \rightarrow 2CO\ (Boudouard\ )} \\ \mathrm{Rs_2: C + 2H_2 \rightarrow CH_4\ (Methane\ cracking)} \\ \mathrm{Rs_3: C + H_2O \rightarrow H_2 + CO\ (Char\ reforming)} \end{cases} \quad (6)$$

Homogenous reactions:
$$\begin{cases} \mathrm{R_{wgs}: CO + H_2O \longleftrightarrow CO_2 + H_2\ (Water\ gas\ shift)} \\ \mathrm{Rg_1: CH_4 + H_2O \longleftrightarrow 3H_2 + CO\ (Methane\ reforming)} \end{cases} \quad (7)$$

Kinetic rates of these reactions are taken from several published papers as shown in Table 2.

2.3 Governing equations

The governing equations for the 1D steady-state model are the solid and gas phase differential mass and heat balances:

Conservation of species:

Solid phase: $\frac{\partial(u_s\rho_i)}{\partial z} = +\sum_{k=1}^{nr,i} R_{k,i}\ \ (i = Biomass, Moisture, Ash, C)$, k = reaction number (8)

Gas phase: $\frac{\partial(\varepsilon u_g\rho_i)}{\partial z} = +\sum_{k=1}^{nr,j} R_{k,j}\ \ (j = H_2O, H_2, CH_4, CO, CO_2, Tar, \dots)$ (9)

Energy Balance:

Solid phase: $\sum_{i=1}^{ns} R_{k,i}\ \ \frac{\partial(u_s\rho_i cp_i Ts)}{\partial z} = +\sum_{k=1}^{nrs}(-\Delta H_k)\cdot\ R_k - (Q_{sg} + Q_{sw})$ (10)

Gas phase: $\sum_{j=1}^{ng} R_{k,j}\ \ \frac{\partial(\varepsilon u_g\rho_j cp_j Tg)}{\partial z} = +\sum_{j=1}^{nrg}\left(-\Delta H_{k,l}\right)\cdot\ R_{k,l} - (-Q_{sg} + Q_{gw})$ (11)

Continuity:

$$u_s = +u_{s,0}\ ; \qquad \sum\frac{\partial(u_g\rho_j)}{\partial z} = +\sum_{j=1}^{nrg} R_{k,l} \quad (12)$$

Due to the assumptions, the set of mass, heat and continuity equations must be coupled with the following thermodynamics relations:

$$\sum_{j=1}^{gas}\frac{\rho_{g,j}}{M_g} = \frac{P}{RT_g}\ ; \qquad cp_s\ = \sum_{i=1}^{solid}\frac{\rho_{s,i}}{\rho_s}\cdot cp_{s,i}\ ; \qquad cp_g\ = \sum_{j=1}^{gas}\frac{\rho_{g,j}}{\rho_g}\cdot cp_{g,j} \quad (13)$$

The model supposes that no spatial intra-particle gradients of temperature exist, particles are spherical and have the same size, and the porosity of the bed remains constant. The momentum balance is not considered to simplify. The reactor is thus supposed to work in isobaric conditions. In the solid phase continuity equation, u_{s0} is the initial velocity of the solid flow. This is possible because, for

assumption, the particle's external diameter does not change, as a consequence $dp = dp_0$ and ε = constant. Correlations were taken from existing literature regarding the solid/gas heat transfer and the mass transfer coefficients [31]: $A_{sg}=6(1-\varepsilon)/dp_0$ is the particle density number; $h_{sg}=2.06\, u_g \rho_g\, cp_g\, Re^{-0.575}\, Pr^{-2/3}$ is the solid/gas heat transfer coefficient. The experimental correlation is multiplied by empirical factors (ζ) with values in the range 0.02-1 [35]. $Q_{sg}=\zeta \cdot h_{sg} \cdot A_{sg} \cdot (Ts-Tg)$ is the convective term for heat-mass transfer between phases, and $Q_{sg,w}$ is the gas/solid to wall heat-mass transfer terms [24].

It is important to specify that the total mass production rate, $\sum R$, comprehends both heterogeneous and homogenous reactions for a generic gas species, whilst referring only to solid-gas reactions when computing solids rates of production. Specific heating values (Cp_i) of the species were combined with sensible enthalpies to obtain a comprehensive formulation, as suggested in [36]. Only specific heat of tar and ashes were supposed to be constant and taken from the literature [27].

2.3.1 Solar Irradiation

To simulate an external solar source contribution a radiative transfer term must be added in the governing equations. In this study the external source modelling proposed by *Belghit et al.*[37] is implemented. In detail, the bed of the reactor can be modelled as an optically thick grey medium defined by two key parameters: emissivity, ξ_{bed} and extinction coefficient, *Ex*. The irradiance or radiative flux density is a measure of the amount of radiation received by an object from a given source and approximated by the Rossland's formulation [38] as:

$$q_r(z) = \frac{-16\sigma T^3}{3Ex} \cdot \frac{\partial T}{\partial z} \tag{14}$$

$$\frac{\partial q_r(z)}{\partial z} = \frac{+16\sigma T^3}{3Ex}\frac{\partial^2 T}{\partial z^2} - \frac{16\sigma T^2}{Ex}\left(\frac{\partial T}{\partial z}\right)^2 \tag{15}$$

The term $\frac{-16\sigma T^3}{3Ex}$ represents radiative conductivity (λ_r), while σ is the Stefan–Boltzmann constant. Since the solid bed is directly irradiated by a concentrated solar flux, it is subjected to a noteworthy thermal gradient; as a consequence, thermal conductivity must be introduced in the model through the second derivative of temperature and an effective thermal conductivity λ_s^*. In absence of experimental data, this last parameter is taken from a range of 0.1 to 0.9 *W/m K* as found empirically for porous carbonaceous feedstocks [39]. Finally, the energy balance of the solid phase (10) was reshaped including a second derivative term and irradiance contribution:

$$\sum_{i=1}^{ns} R_{k,i}\ \frac{\partial(u_s \rho_i cp_i T_s)}{\partial z} = \frac{\partial}{\partial z}\left[\lambda_s^* \frac{\partial T_s}{\partial z}\right] - \frac{\partial q_r(z)}{\partial z} + \sum_{k=1}^{nrs}(-\Delta H_k) \cdot\ R_k - (Q_{sg} + Q_{sw}) \tag{16}$$

The boundary condition for obtaining a steady-state solution is represented by the temperature of the solid phase at *z=0*, Ts_0, acting as a "warm-front". This initial temperature is related to the net incidental solar flux *J*, expressed by means of a local thermal balance at the irradiated region:

$$\alpha_g \cdot J = \sigma \cdot \xi_{bed} \cdot \left(T_{s,0}^4 - T_{g,0}^4\right) - \lambda_s^* \cdot \left.\frac{\partial T_s}{\partial z}\right|_0 \quad (17)$$

Where α_g is the absorptivity of solid particles. This relationship permits to obtain the initial solid temperature for a chosen net solar flux and vice versa.

2.4 Process efficiency analysis

The upgrade factor or chemical conversion efficiency, *U*, will be analysed for each of the gasification methods evaluated. It will be determined from the ratio between the calorific value of producer gas over feedstock and it represents the most intuitive performance parameter to assess quality and quantity of syngas produced:

$$U = \frac{m_{syngas}\ LHV_{syngas}}{m_{biomass}\ LHV_{biomass}} \quad (18)$$

Regarding the solar-driven gasification, several different scenarios of solar radiation flux are analysed and their impact on the main performance indicators assessed. The measure of how good the sun energy input is converted into chemical energy for syngas production will be through the energy conversion efficiency, η, defined as

$$\eta = \frac{m_{syngas}\ LHV_{syngas}}{Q_{solar} + m_{biomass}\ LHV_{biomass}} \quad (19)$$

Where Q_{solar} is the total solar energy delivered through the receiver aperture. This can be determined after fixing a working temperature inside the reactor and then calculating the solar flux. The net power absorbed in the solar reactor can be approximated as equal to Q_{solar} and it must match the total enthalpy change of the reaction. i.e.

$$Q_{solar} = \dot{n}\Delta H|_{Reactants\ @\ Initial\ Temperature \rightarrow Products\ @\ Final\ Temperature}$$

2.5 Input parameters

The model developed is fully scalable. However, the simulation results presented in the next sections referring to a reactor with the characteristics tabulated in Table 3. The diameter of the reactor is 1.5m as suggested by Basu [19] with an optimal height of the bed taken according to [45]. A consumption rate of 500 kg/hr is chosen to simulate an industrial plant. For the solar reactor, a larger plant should even have even less re-radiation losses than the heat losses according to [11] by virtue of having a larger bed surface area. This helps to mitigate the influence of neglecting losses inside the reactor. The gas and solid initial temperatures were varied accordingly, and a number of simulations were run to analyse the system's behaviour and to find optimal input/output.

2.6 Numerical solution

The numerical programme to solve the system of ordinary differential equations (ODEs) above was developed and implemented on MATLAB. Initially, the input parameters such as fuel characteristics,

reactor's geometry and gasifying agent quantity and temperature are read. For the solar gasifier model, the radiative energy flux is a fundamental entry to calculate the initial solid phase temperature. Eventually, the ODEs are solved and integrated using MATLAB's *"ode23s"* function. The "ode23s'' algorithm is an implicit one-step algorithm based on a second order modified Rosenbrock's formula [40] and it is particularly suited for 'stiff' problems [41]. The reactor is then divided into elementary cylindrical cells of cross section equal to reactor's diameter and height of steps of 10^{-3}m (z direction). At each iteration step, starting from an initial state (e.g. concentrations and temperature in both phases), the differential equations are solved simultaneously with the material and heat balances. The numerical solution convergence was obtained when all the main variables had residuals < 10^{-6}.

3 Results and discussion

3.1 Autothermal reactor with steam injection

The drying, pyrolysis and combustion effect on the feedstock can be appreciated by analysing the partial density plot presented in Figure 2. From z/H=0 to z/H=0.1 biomass starts to deplete and release gases due to pyrolysis. After this point, at z/H=0.11, the concentration of oxygen plummets due to the partial combustion and the gasification reactions start to work at full regime.

The numerical solutions for producer gas composition have been evaluated using an optimal ER value equal to 0.25 and a steam to carbon ratio of 1/8, obtained by trial and error. The results were compared with experimental results of similar carbonaceous feedstock, and they are reported in Table 4.

The dry syngas mainly consisted of CO, 37%, followed by Hydrogen, 30.4% and CO_2, 25%. CH_4 was present in a small quantity (6%) due to the high gasification temperatures which stop the methane reforming reaction as already reckoned by other authors [24,25,42,43]. The lower heating value of the producer gas obtained was calculated 9.95 MJ/Kg and the conversion process efficiency, *U*, was near to 65%.

These results are in substantial agreement to Jordan's work [19], where the sugar cane bagasse characteristics were taken. For instance, CO accounted for 35% or 2% less than the value registered in our study. The methane output was also matched, with 6.4% and 7% respectively. The slight difference in Jordan's H_2 and CO_2 content can be explained by the different optimal parameters used for ER and steam injection quantity used to obtain average values from different experimental runs.

Comparing the results with [42] we notice how generally the simulation is in good agreement regarding species concentration, that are within a ±4 % range. The small differences in the output can be easily addressed by noticing the differences in the type and particles size of the biomass utilised (wood chips of 3-5cm diameter). This can have a non-negligible effect on surface reaction mechanics.

3.2 High temperature air gasification

The HTAG process was simulated for a mixture of air/steam preheated up to 1500K as in Wu et al. [9,18]. The gas obtained was highly characterised by the presence of CO and H_2 representing, respectively, 48% and 30% of the syngas (Table 4). Due to the high temperature developed in the gasifier the carbon dioxide production was limited, accounting for no more than 15%. The efficiency of the thermal process was at its maximum for $T_{steam=}$1500K, reaching 81% with a syngas LHV of 10.27 MJ/kg. The heavily preheated gasification agent is able to reach a very high temperature in the reactor thanks to partial combustion. Although the temperature reached is higher than that in the auto-thermal case, the partial combustion is not affected by any means since the only parameters affecting it is the E.R. The principal effect of the injected hot air/steam is to anticipate the partial combustion and thus allow a higher gasification temperature in the plant to be reached.

Experimental results on a downdraft HTAG plant are limited in the literature, however the model developed is revealed to be in good agreement with the work of Wu et al.[18], as shown Table 4. The yield of H_2 and CO is a very good match, within a ±1.1% range. A difference of 5.5% can be noticed in the CO_2 output, which is higher in the experimental results. These differences in the syngas composition value may be caused by the different biomass used in the aforementioned study combined with a different steam injection quantity.

3.3 High temperature steam gasification

From the temperature profile reported in Fig.3 the highly endothermic character of Steam Gasification can be appreciated. In the downdraft configuration, supplying heat through steam is revealed to be an inefficient way to produce gasification temperature in such reactor type. In fact, temperature drops can be noticed due to the limited capacity of the steam as a thermal carrier. Injecting a super preheated water vapour at 1400K creates a solid bed profile and a gasification temperature of nearly 1050K. Therefore, the syngas production is lower in quantity with respect to the other gasification technologies and the overall efficiency is limited to a max of 35% (Table 4). This is mainly caused by the scarcity of CO produced by the char gasification reaction, which is not efficiently exploited at temperatures <1200K. The limited efficiency is also caused by the presence of Tars (around 7.5%) in the end gas due to the absence of tars-cracking provided by combustion reactions.

However, the steam-only gasification is able to shift the syngas production towards an H_2 rich gas (>50% in the end gas) with good LHV values. A key parameter is represented by the S/C as shown in Table 4. Optimal production was computed at S/C=1.5, with a syngas LHV value of 13MJ/Kg and a composition of 55.6% H_2, 11.1% CO, while the CO_2 presence was of 26.5%. This particular technology appears to be a good candidate for hydrogen production. However, the co-current

gasification configuration is not the most adaptive, and higher gas yield or thermal efficiency can be achieved using a counter-current or updraft configuration as proposed and experimented in [7,11,17]. Nevertheless, the results appear to be in good agreement with updraft HTSG gasificator experimented by Umekias as well as with the temperature profiles, compared in Figure 3. The temperature at the distance z/H=0 represents the injected steam temperature and since the biomass is heated only by high temperature steam a sharp drop is registered along the gas flow direction. This allows the heat exchange between the biomass solid phase and the steam, thus starting the gasification reactions.

The effects of the Steam/Carbon ratio can be seen in Fig.4. Overall, incrementing the content of steam in the gasification process enhances the hydrogen production while decreasing CO. However, the maximum process efficiency is found to be at S/C=1. Further incrementing the H_2O content gradually saturates the gas in the reactor and causes the consequent boost of the water gas shift reaction, which dominates with respect to all the other reactions in these lower working temperatures, eventually transforming most of the CO into CO_2 and H_2. Although this enhances the H_2 content, it also results in an undesired over production of CO_2 which is denser than hydrogen. As a consequence, syngas quantity goes down as well as the system efficiency.

All the syngas species resulted to be within a ±4% range with respect to the experimental value in [17]. A lower efficiency of 35% versus 55% is easily explained considering that an updraft configuration, as in Umeki's, is generally more efficient for industrial scale plants [1].

3.4 Solar-driven gasification

The solar-driven gasification process was related to one key parameter, the net solar flux (***J***) at the entrance of the reactor chamber. A reference value of ***J*** was taken as $\boldsymbol{J_o} = 2.165 \cdot 10^5$ W/m^2 corresponding to a constant highly concentrated net solar flux required to heat up the solid bed to 1400K. This flux density value, obtained through a thermal balance at the reactor entrance, is in agreement with other studies [3,37]. For instance, in [44] the energy flux was around 0.4-0.8 MW/m^2 , in [45] it was brought up to 1 MW/m^2 and a value of 0.5 MW/m^2 was used in [46]. If we consider that generally 50% of the solar radiation is lost, we reach a reference value of $2 \cdot J_o$ = 0.433 MW/m^2 which matches the range of values presented in the other studies. The initial temperature of the gas phase was set to 300K, the extinction rate, *Ex*, and the effective conductivity of the bed, $\boldsymbol{\lambda^*_s}$, were calculated for each case.

The allothermal solar gasification performance was investigated for a range of solar inputs and the results are presented in Figure 5 and Figure 6 with the steam flow at the reactor entrance. The ratio of steam quantity, as shown in Figure 5, injected in the reactor directly influences the H_2 production as widely recognised in the literature [8,11,16,47]. However, a relatively high S/C ratio also increases the CO_2 production due to the water-gas shift reaction saturation and a consequent CO consumption.

For this solar reactor of biomass, the optimal S/C value was calculated to be 0.5. The biomass sample already contains around 10% of moisture and, as a consequence, it would require less steam to be injected than a dry feedstock. The solar input J was revealed to have had a strong impact on the gasification products due to the higher reactor temperature that is achievable. As J augments, so the carbon monoxide generation increases. Conversely, due to the improved char gasification reaction, CO_2 is kept low. However, at S/C = 0.5 and starting from $J=3\times J_{0,}$ the H_2 production starts to stall in correspondence of when its concentration becomes very close to that of CO and then reaches the thermodynamic equilibrium composition. The water-gas shift reaction is sensitive to temperature, and the higher temperature, the higher the tendency to shift towards reactants production due to Le Chatelier's principle. Thus the WGS stalls while the other reactions, enhanced by high temperatures, guarantee a constant production of CO in the producer gas. Thus, it appears to present a limit in the solar input after which the H_2 output does not change substantially. This particular behaviour corroborates with the study of [46].

The steady state temperature profiles are reported in Fig.6. The temperature inside the reactor is supported by the constant solar heating flux, at the reactor's entrance, which sustains the endothermic gasification reactions. Due to the particular gasification technology and reactor design, no validation of temperature profile is possible. However, the gradual drop in temperature along the bed appears to be consistent with the behaviour of traditional fixed bed / downdraft gasifiers.

The solar gasification results at $J=J_0$ are compared with those of the experimental study of Kruesi [42] who used a solar reactor in a "drop-tube" configuration with a sugar cane bagasse as fuel. It is apparent from this comparison that the model results are in agreement with the empirical study. The efficiency of the solar process, η, was calculated in the same way in both these studies, however it appears the value obtained by simulation is nearly double. This may be due to the fact that the present study neglected the thermal losses in the reactors, which usually account for around 50% of the total energy input [39,49]. Furthermore, according to [16] larger diameter reactors achieve higher reaction rates for the same radiative power leading to a higher overall solar-to-fuel efficiency.

Solar gasification Upgrade factor dependency on solar input and steam/carbon ratio is showed in Figure 7. It is evident that the higher the solar input, the more energy is stored in syngas. Secondly, the upgrade factor and thus the LHV of the syngas was found to be indirectly proportional to the amount of water vapour injected in the reactor. This is mainly due to the excess water causing a steep increase in CO_2 production not matched by an analogue H_2 increment. Theoretically, higher upgrade factors are possible under the 0.5 S/C ratios, however these would not be feasible in reality due to the impossibility to drive gasification reactions without sufficient steam injections.

3.5 Performance comparison

A direct comparison among the different steam-gasification technologies examining their performance characteristics is reported in Figure 8 and Figure 9. It is evident in Figure 8 that the different technologies have different syngas outputs for the same feedstock and operative conditions, thus they may have different applications.

Generally, solar gasification seems to be the most promising method to obtain a very high quality syngas, rich in H_2 and CO and low in carbon dioxide emissions. The solar-driven gasification results presented for the comparison are those obtained by using $J=J_0$ as a solar input, and thus are not the optimal outputs as already shown in Figure 5. Nevertheless, the producer gas stands highest for both LHV value and quantity produced, with an upgrade factor *U* of 118%. In other words, the sugar bagasse was solar upgraded for a factor of 18%. Thus, the solar process was found to be very efficient with the lowest CO_2 production (<15%).

A good quality syngas, mostly composed by hydrogen, is also achievable with the HTSG process. In fact, the H_2 yield was of 55% with CO accounting for 10%. However, the large amount of CO_2 produced, about 28%, makes the thermal process efficiency the lowest of the group, settling at 35%. This is principally caused by the poor efficiency of the co-current high temperature steam-only gasification, which can be improved using an updraft configuration. Having said that, this technology seems to be the most promising for pure hydrogen production, especially with a CO_2 capture / absorbent method.

Using a highly preheated air/steam mixture (HTAG) can improve the traditional gasification process. In fact, the higher temperature of the gasification agent greatly improves the pyrolysis and gasification rates. This results in improved thermal conversion rates compared to the auto-thermal process, with rates of 80% versus 65%, respectively. As a consequence, the CO production rose to 48% from 38% with CO_2 dropping by more than 10%. However, the energy expenditure necessary to preheat the gasification agent to such high temperatures should be duly taken in account.

A comparison of the temperature profiles of the different gasification mechanism is presented in Figure 9. For the non-solar technologies, temperature profiles' behaviour along the bed and after pyrolysis appear to be similar due to both similar fuel properties and model assumptions. Differences can be found between gas and solid phase profiles at the reactor entrances. In the HTSG reactor, the temperature drop is the most severe due to the high quantity of steam utilised and consequent heating absorption. Conversely, in the HTAG gasification the temperature inside the reactor is higher due to the already preheated steam, which limits temperature drops and enhances the gasification reactions. In solar gasification, the thermal transfer acts differently due to the bed thermal conductivity and extinction rate, causing a different gas phase profile in the reactor.

3.6 Limitations of the model

The 1-D numerical model presented in this paper was utilized to run simulations for a cylindrical shaped fixed-bed reactor. The design parameters were in common for each technology and taken from optimal values present in literature. However, in a real working environment, the time factor might not be neglected. Gas production quality may be not continuous due to temperature fluctuations of both solid phase and gasifying agent. For the solar gasifier, the solar input consistency is crucial, and the overall process efficiency should be considered only at the end of a full working period. Reactor design parameters may play a major role on heat/mass exchange modes characteristic times. In terms of syngas production over time, the conclusions of which gasification technology is the most efficient and convenient may be slightly different respect to the steady-state.

The particles size, *dp,* also plays a fundamental role in a steam gasifier performance as they directly affect the actual heating rates during pyrolysis and gasification time. In general, particle's size may affect the rate of devolatilisation, influencing the time required for the overall gasification process, independently from the technology used [19,24]. In the literature cited in this article, the optimal particles size for biomass is usually reported in the range of 10-10000μm. The HTAG revealed to be the most insensitive to particle size variations [18]. In the solar driven reactor decreasing particle's diameter will increase the contact area, improving heat exchange by a more rapid radiation absorption, as well as conversion efficiency [3,37]. The effect of particle size issue could be addressed by using more ad-hoc pyrolysis models.

A future work may be focused on developing optimal reactor's design for each of the steam gasification technologies. This can be achieved implementing an optimization routine in MATLAB, where the system of differential equations will be solved iteratively for each gasification method and for a number of realistic reactor geometries. In a second step, time derivatives may be implemented in the numerical model, to compute and compare the gas productions in fixed periods of time. This will allow to further enhance the discussion regarding pro and contra of each technology, especially their economic viability.

4 Conclusion

A computational model of a biomass downdraft chemical reactor using both auto-thermal and allo-thermal technologies has been presented. The multi-purpose kinetic model allows the determination of producer gas composition as well as gas and solid temperature profiles along the reactor as function of functional parameters.

Despite the modelling assumptions and limitations, the model proposed was found to be robust enough and able to return products of different gasification technologies with a good grade of accuracy with respect to the experimental results. A direct comparison of advantages and disadvantages of each is also provided by the model that can work on multi-task. A higher sophistication of the model will more than likely only have a limited effect on producer gas composition prediction.

Without using complex 3D modelling, this comprehensive 1-D model can reasonably be used to assess and analyse the gasification performances of varying gasification approaches, and appears to be especially suitable for gasification agents with additional heat sources. In particular, the proposed model examined in this work has been able to predict:

1. Steam gasification efficiency and products that are highly influenced by the steam/carbon ratio. Optimal set ups must be found for each gasification technology. Although increasing steam injection after a certain optimal value enhances the syngas quality, it can also be counterproductive.
2. Solar gasification using steam as a gasification agent proved to be the most efficient way to convert biomass into high quality gas. Increasing the solar input would increase the rate of gasification chemical reactions, subsequently increasing gas and solid phase temperatures. An optimal value of the solar input can be found, after which there are no further noticeable improvements in the results. Eventually, the solar driven gasification results in us being able to produce the syngas with a) the highest LHV and Upgrade factor; b) lowest amount of CO_2;
3. The High Temperature Agent Gasification (HTAG) can be used to improve a conventional auto-thermal reactors' efficiency and syngas output.
4. High Temperature Steam Gasification (HTSG) appears to be the best method to produce a producer gas extremely rich in H_2. However, its process conversion efficiency was found to be the lowest.

Bibliography

[1] Basu P. Biomass Gasification and Pyrolysis: Practical Design and Theory. Academic Press; 2010.

[2] Ruiz J a., Juárez MC, Morales MP, Muñoz P, Mendívil M a. Biomass gasification for electricity generation: Review of current technology barriers. Renew Sustain Energy Rev 2013;18:174–83. doi:10.1016/j.rser.2012.10.021.

[3] Belghit A, Daguenet M, Reddy A. Heat and mass transfer in a high temperature packed moving bed subject to an external radiative source. Chem Eng Sci 2000;55:3967–78.

[4] Kodama T, Kondoh Y, Tamagawa T, Funatoh A, Shimizu K-I, Kitayama Y. Fluidized Bed Coal Gasification with CO2 under Direct Irradiation with Concentrated Visible Light. Energy & Fuels 2002;16:1264–70. doi:10.1021/ef020053x.

[5] Gokon N, Ono R, Hatamachi T, Liuyun L, Kim H-J, Kodama T. CO2 gasification of coal cokes using internally circulating fluidized bed reactor by concentrated Xe-light irradiation for solar gasification. Int J Hydrogen Energy 2012;37:12128–37. doi:10.1016/j.ijhydene.2012.05.133.

[6] Piatkowski N, Wieckert C, Weimer AW, Steinfeld A. Solar-driven gasification of carbonaceous feedstock, a review. Energy Environ Sci 2011;4:73. doi:10.1039/c0ee00312c.

[7] Umeki K, Son Y, Namioka T, Yoshikawa K. Basic Study on Hydrogen-Rich Gas Production by High Temperature Steam Gasification of Solid Wastes. J Environ Eng 2009;4:211–21. doi:10.1299/jee.4.211.

[8] Valliyappan T, Ferdous D, Bakhshi NN, Dalai a. K. Production of hydrogen and syngas via steam gasification of glycerol in a fixed-bed reactor. Top Catal 2008;49:59–67. doi:10.1007/s11244-008-9062-7.

[9] Wu Y, Yang W, Blasiak W. Energy and Exergy Analysis of High Temperature Agent Gasification of Biomass. Energies 2014;7:2107–22. doi:10.3390/en7042107.

[10] Mhilu CF. Modeling Performance of High-Temperature Biomass Gasification Process. ISRN Chem Eng 2012;2012:1–13. doi:10.5402/2012/437186.

[11] Umeki K, Yamamoto K, Namioka T, Yoshikawa K. High temperature steam-only gasification of woody biomass. Appl Energy 2010;87:791–8. doi:10.1016/j.apenergy.2009.09.035.

[12] Skoulou V, Kantarelis E, Arvelakis S, Yang W, Zabaniotou a. Effect of biomass leaching on H2 production, ash and tar behavior during high temperature steam gasification (HTSG) process. Int J Hydrogen Energy 2009;34:5666–73. doi:10.1016/j.ijhydene.2009.05.117.

[13] Wieckert C, Obrist A, Zedtwitz P von, Maag G, Steinfeld A. Syngas Production by Thermochemical Gasification of Carbonaceous Waste Materials in a 150 kWth Packed-Bed Solar Reactor. Energy & Fuels 2013;27:4770–6. doi:10.1021/ef4008399.

[14] Kruesi M, Jovanovic ZR, dos Santos EC, Yoon HC, Steinfeld A. Solar-driven steam-based gasification of sugarcane bagasse in ad experimental analyses. Biomass and Bioenergy 2013;52:173–83. doi:10.1016/j.biombioe.2013.03.003.

[15] Puig-Arnavat M, Tora E a., Bruno JC, Coronas a. State of the art on reactor designs for solar gasification of carbonaceous feedstock. Sol Energy 2013;97:67–84. doi:10.1016/j.solener.2013.08.001.

[16] Piatkowski N, Steinfeld A. Solar Gasification of Carbonaceous Waste Feedstocks in a Packed-Bed Reactor: Dynamic Modeling and Experimental Validation 2011;57. doi:10.1002/aic.

[17] Umeki K, Namioka T, Yoshikawa K. Analysis of an updraft biomass gasifier with high temperature steam using a numerical model. Appl Energy 2012;90:38–45. doi:10.1016/j.apenergy.2010.12.058.

[18] Wu Y, Zhang Q, Yang W, Blasiak W. Two-dimensional computational fluid dynamics simulation of biomass gasification in a downdraft fixed-bed gasifier with highly preheated air and steam. Energy and Fuels 2013;27:3274–82. doi:10.1021/ef4003704.

[19] Jordan CA. Intesidifed gasification of fuel cane bagasse for power production using solid-oxide fuel cells. 2011.

[20] Krusi M. Heat transfer enhancement in a solar biomass gasifier. Int J 2011;2:1–4.

[21] Carvalho-Netto O V, Bressiani JA, Soriano HL, Fiori CS, Santos JM, Barbosa GV, et al. The potential of the energy cane as the main biomass crop for the cellulosic industry. Chem Biol Technol Agric 2014;1:20. doi:10.1186/s40538-014-0020-2.

[22] Raza SS, Janajreh I. Solar Assisted Gasification of Solid Feedstock: Optical Arrangement and Numerical Simulation 2014;7:65–72. doi:10.5383/ijtee.07.02.002.

[23] Gregg DW, Taylor RW, Campbell JH, Taylor JR, Cotton A. Solar gasification of coal,actived

carbon,coke and biomass mixture 1980;25.

[24] Blasi C Di. Dynamic behaviour of stratified downdraft gasifiers. Chem Eng Sci 2000;55.

[25] Souza-Santos ML. Solid Fuels Combustion and Gasification Modeling, Simulation, and Equipment Operation. 2nd ed. CRC Press; 2004.

[26] Di Blasi C. Modeling wood gasification in a countercurrent fixed-bed reactor. AIChE J 2004;50:2306–19. doi:10.1002/aic.10189.

[27] Mandl C. Modelling of an updraft fixed-bed gasifier operated with softwood pellets. Fuel 2010;89:3795–806.

[28] Santos EC dos. Solar gasification of sugarcane bagasse : thermogravimetric analysis of the kinetics of pyrolysis and steam gasification. n.d.

[29] Danaei Kenarsari S, Zheng Y. Fast Pyrolysis of Biomass Pellets Using Concentrated Solar Radiation: A Numerical Study. J Sol Energy Eng 2014;136:41004.

[30] Antal MJ, Hofmann L, Moreira J, Brown CT, Steenblik R. Design and operation of a solar fired biomass flash pyrolysis reactor. Sol Energy 1983;30:299–312. doi:http://dx.doi.org/10.1016/0038-092X(83)90185-8.

[31] Hobbs ML, Radulovic PT, Smoot LD. Modeling Fixed-Bed Coal Gasifiers 1992;38:681–702.

[32] Park KY, Edgar TF. Modeling of early cavity growth for underground coal gasification. Ind Eng Chem Res 1987;26:237–46. doi:10.1021/ie00062a011.

[33] Wen CY, Chaung TZ. Entrainment Coal Gasification Modeling 1979;18:684–95.

[34] Kayal TK, Chakravarty M. Mathematical modelling of steady state updraft gasification of jute stick particles of definite sizes packed randomly. Bioresour Technol 1997;60:131–41.

[35] Hobbs ML, Radulovic PT. Combustion and gasification of coals in fixed beds 1994;19:505–86.

[36] Reid Sherwood, Thomas K., RC. The properties of gases and liquids: their estimation and correlation. New York: McGraw-Hill; 1966.

[37] Belghit A, Daguenet M. Study of heat and mass transfer in a chemical moving bed reactor for gasification of carbon using an external radiative source 1988;32:2015–25.

[38] Rosseland S. Theoretical Astrophysics. London: Oxford University Press; 1936.

[39] Piatkowski N, Steinfeld A. Solar-Driven Coal Gasification in a Thermally Irradiated Packed-Bed Reactor. Energy & Fuels 2008;22:2043–52. doi:10.1021/ef800027c.

[40] Rosenbrock HH. Some general implicit processes for the numerical solution of differential equations. Comput J 1963;5:329–30. doi:10.1007/s13398-014-0173-7.2.

[41] Shampine LF, Reichelt MW. The MATLAB ODE Suite. SIAM J Sci Comput 1997;18:1–22. doi:10.1137/S1064827594276424.

[42] Jayah TH, Aye L, Fuller RJ, Stewart DF. Computer simulation of a downdraft wood gasifier for tea drying. Biomass and Bioenergy 2003;25:459–69. doi:10.1016/S0961-9534(03)00037-0.

[43] Zainal Z a., Rifau A, Quadir G a., Seetharamu KN. Experimental investigation of a downdraft biomass gasifier. Biomass and Bioenergy 2002;23:283–9. doi:10.1016/S0961-9534(02)00059-4.

[44] Zgraggen A, Haueter P, Trommer D, Romero M, Dejesus J, Steinfeld A. Hydrogen production by steam-gasification of petroleum coke using concentrated solar power: II Reactor design, testing, and modeling. Int J Hydrogen Energy 2006;31:797–811. doi:10.1016/j.ijhydene.2005.06.011.

[45] Kodama T, Gokon N, Enomoto S, Itoh S, Hatamachi T. Coal Coke Gasification in a Windowed Solar Chemical Reactor for Beam-Down Optics. J Sol Energy Eng

2010;132:41004.

[46] Xu J, Qiao L. Solar Coal Gasification Modeling in a Well-Stirred Reactor with Detailed Gas-Phase Chemistry 2012:1–11.

[47] Inayat A, Ahmad MM, Yusup S, Mutalib MIA. Biomass Steam Gasification with In-Situ CO2 Capture for Enriched Hydrogen Gas Production: A Reaction Kinetics Modelling Approach. Energies 2010;3:1472–84. doi:10.3390/en3081472.

[48] Kruesi M, Jovanovic ZR, Steinfeld A. A two-zone solar-driven gasifier concept: Reactor design and experimental evaluation with bagasse particles. Fuel 2014;117:680–7. doi:10.1016/j.fuel.2013.09.011.

[49] Piatkowski N, Wieckert C, Steinfeld A. Experimental investigation of a packed-bed solar reactor for the steam-gasification of carbonaceous feedstocks. Fuel Process Technol 2009;90:360–6. doi:10.1016/j.fuproc.2008.10.007.

Nomenclature

$A_i = pre - exponential\ factor\ of\ reaction\ (s^{-1})$

$D_i =\ species\ diffusivity\ (m^2 s^{-1})$

C_i = *Species concentration (kmol* m^{-3}*)*

$cp_i = Specific\ heat\ \ (J\ kg^{-1}\ K^{-1}\ )$

dp_0 = *Particle diameter (m)*

d_c= *inner core diameter (m)*

$E_i = activation\ energy\ of\ reaction\ i\ (J\ mol^{-1})$

Ex = *Extinction coefficient (*m^{-1}*)*

H= bed height (m)

$J =\ Net\ solar\ flux\ (W\ m^{-2})$

$K_i = Kinetic\ reaction\ rate\ (m\ s^{-1})$

$M_i = molar\ weight\ (kg\ mol^{-1})$

$m = Mass\ flow\ rate\ (kg\ s^{-1})$

$P_i = partial\ pressure\ of\ specie\ i\ (Pa)$

Pr = Prandtl number

$q_r = Radiative\ flux\ density\ \ (W\ m^{-2}\ )$

$Q_{solar} = Concentrated\ thermal\ radiation\ (W\ m^{-2})$

Q_{sw}, Q_{gw} = *solid-wall and gas-wall heat transfer terms*

$Rs_i = Solid - gas\ reaction\ rate\ (kg\ m^{-3} s^{-1})$

$Rg_i = Gas - gas\ reaction\ rate\ (kg\ m^{-3} s^{-1})$

$R = Universal\ gas\ constant\ (J\ mol^{-1}\ K^{-1})$

$Sc_i = Schimidt\ number$

T = Temperature (K)

$u_g = gas\ velocity\ (ms^{-1})$

U = gasification upgrade factor.

z = reactor's axial direction

Greek symbols

$\alpha_g = absorptivity\ of\ the\ solid\ particles$

$\Delta H =\ Reaction\ specific\ enthalpy\ (J\ kg^{-1})$

$\varepsilon = void\ fraction$

$\rho = density\ (kg\ m^{-3})$

$\varphi = combustion\ factor$

$\mu_g = dynamic\ viscosity\ (Pa\ s)$

ζ = *Bed reactivity factor*

σ = *Stefan Boltzmann constant (W* m^{-1} K^{-4} *)*

ξ_{bed}= *Solid bed emissivity*

λ_s^* = *effective thermal conductivity* $(W\ m^{-2}K)$

η =*Process efficiency*

TABLE 1: PRODUCTS (MASS %) FROM THE PYROLYSIS REACTIONS IN EQNS. (3,4)

Pyrolysis products expressed in weight/weight							
	CO	**CO_2**	**H_2O**	**CH_4**	**H_2**	**Tar**	**Char**
Rp1	4.5	10	11.5	0.3	0.2	48	25.5
Rp2	53.4	8.5	17	21.1	-	-	-

TABLE 2: REACTION CHEMICAL KINETICS

Reaction	**Kinetic reaction (production) rate (kg/m^3s^{-1})**	***ΔH***	**Source**
R_{dry}	$\rho_{biomass} \cdot 5.56 \cdot 10^6 \exp\left(\frac{-8.79 \cdot 10^4}{RTs}\right)$	+2250 kJ/kg	[27]
R_{pyro1}	$\rho_{biomass} \cdot 10^{4.03} \exp\left(\frac{77.8 \cdot 10^3}{RTs}\right)$	+350 kJ/kg	[27]
R_{tar}	$\rho_{tar} \cdot 66.3 \cdot 10^3 \exp\left(\frac{-66.3 \cdot 10^6}{RTg}\right)$	0	[27]
Rc_{s1}	$-2.30 \cdot Ts \exp(11100/Ts)$ (m/s)	-111 MJ/kmol	[31]
Rc_{g1}	$1.3 \cdot 10^{14} exp\left(\frac{-62.7 \cdot 10^3}{Tg}\right) \cdot [CO][H_2O]^{0.5}[O_2]^{0.5} \left(\frac{kmol}{m^3 s}\right)$	-28.3 MJ/kmol	[25]
Rc_{g2}	$5.26 \cdot 10^{19} \exp\left(\frac{-20.5 \cdot 10^3}{Tg}\right) \cdot [H_2]^{0.85}[C_mH_n]^{-0.56}[O_2]^{1.42} \left(\frac{kmol}{m^3 s}\right)$	-241.7 MJ/kmol	[25]
Rc_{g3}	$2.55 \cdot 10^{17} exp\left(\frac{-11.196 \cdot 10^3}{Tg}\right) \cdot [CH_4][O_2] \left(\frac{kmol}{m^3 s}\right)$	-802.7 MJ/kmol	[25]
Rc_{g4}	$1891.04 \cdot Tg \cdot exp\left(\frac{-12.2 \cdot 10^3}{Tg}\right) \cdot [C_mH_n]^{0.5}[O_2] \left(\frac{kmol}{m^3 s}\right)$	Variable	[25]
R_{s1}	$1.12 \cdot 10^8 exp\left(\frac{-245 \cdot 10^3}{RTs}\right) \cdot P_{co_2}^{0.31}$	+172 MJ/kmol	[17]
R_{s2}	$\frac{6}{dp0} \cdot 20.8 \cdot 10^{-4} exp\left(\frac{-230 \cdot 10^3}{RTs}\right) \cdot [H_2]$	-75 MJ/kmol	[25]
R_{s3}	$2.07 \cdot 10^7 \exp\left(\frac{-220 \cdot 10^3}{RTs}\right) \cdot P_{H_2O}^{0.73}$	+131 MJ/kmol	[17]
$R_{watergas}$	$2.78 \cdot 10^3 \exp(-1513/Tg) \cdot \left([CO] \cdot [H_2O] - \frac{[CO_2] \cdot [H_2]}{0.0256 exp(\frac{3966}{Tg})}\right)$	−41 MJ/kmol	[25]
R_{g1}	$3.1 \cdot 10^3 exp(-15 \cdot 10^3/Tg \cdot \left([CH_4] \cdot [H_2O] - \frac{[CO] \cdot [H_2]^2}{0.0265 \cdot (32.9 \cdot 10^3/Tg)}\right)$	+206 MJ/kmol	[17]

TABLE 3: OPTIMAL OPERATIVE PARAMETERS

PARAMETER	Design Value	Autothermal	HTAG	HTSG	SOLAR
Diameter (m)	1.5	-	-	-	-
Bed height *H* (m)	2.34 m	-	-	-	-
Feeding rate (Kg/s)	0.14	-	-	-	-
Particle diameter *dp* (m)	$6 \cdot 10^{-3}$	-	-	-	-
Bed void fraction ε	0.5	-	-	-	-
Extinction coefficient, *Ex*	10^3 m^{-1}	-	-	-	-
Bed emissivity, ξ_{bed}	0.85	-	-	-	-
Solid initial temperature Ts_i (K)	-	450	300	300	1400
Steam to fuel ratio *S/C*	-	1/8	1/8	1	0.5
Steam temperature T_{steam} (K)	-	300	1500	1400	400

TABLE 4: COMPARISON AND VALIDATION OF DATA WITH DIFFERENT STEAM GASIFICATION PROCESSES

Species in Syngas (%)	**Autothermal-steam gasification (*ER*=0.25) % Total Gas / % Dry Gas (H_2O, N_2 Free)**	**Jordan** [19]	**Jayah** [42]
CO	19.0 / 37.3	17.2/35.4	19.1/40.5
H_2	15.5 /30.4	12.1/24.9	15.5/32.9
CO_2	13.1/25.7	15.8/32.57	11.4/24.2
CH_4	3.3/6.4	3.4/7	1.1/2.3
Efficiency	65%	-	-
	HTAG T_{steam} = 1500K	**Wu *et al.*** [18]	
CO	48.0	46.9	
H_2	30.2	29.1	
CO_2	15.4	21.1	
CH_4	1.0	2.9	
Efficiency	81%	-	
	Downdraft HTSG (S/C = 1.5)	**Updraft HTSG Umeki** [17]	
CO	10.1	13.8	
H_2	55.7	52.5	
CO_2	26.5	30.4	
CH_4	<1	3.0	
Efficiency	35%	55%	

TABLE 5: SOLAR GASIFICATION MODEL PRODUCTS WITH VALIDATION

Properties	**Solar gasification at J_0**	**Kruesi** [48]
H_2 % mol	42.0	45.8
CO % mol	34.0	33.8
CO_2 % mol	14.9	13.2
$LHV_{feedstock} - LHV_{Syngas}$	14.0 – 17.5 MJ/kg	15.9 – 16.5 MJ/kg
U	1.18	1.06
η	41.4 %	21 %

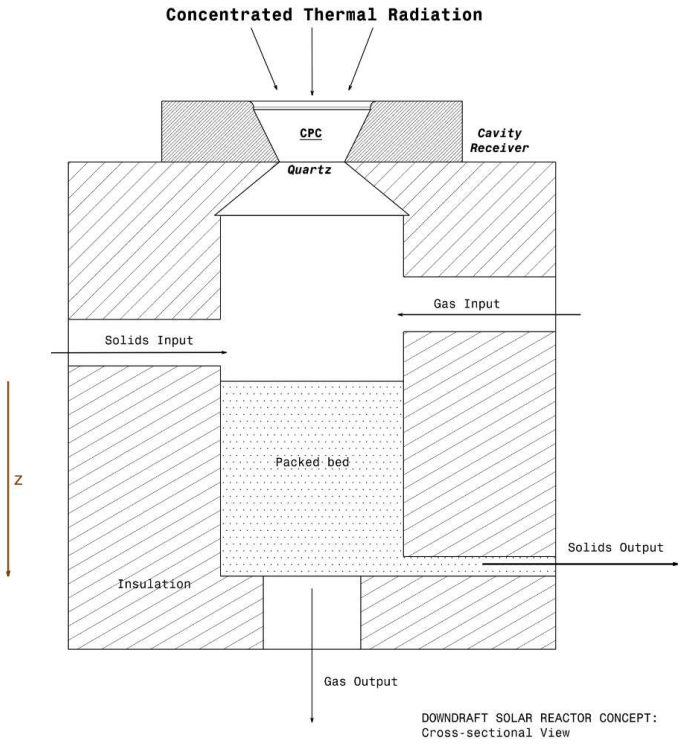

FIGURE 1: SCHEMATIC OF SOLAR GASIFICATION REACTOR

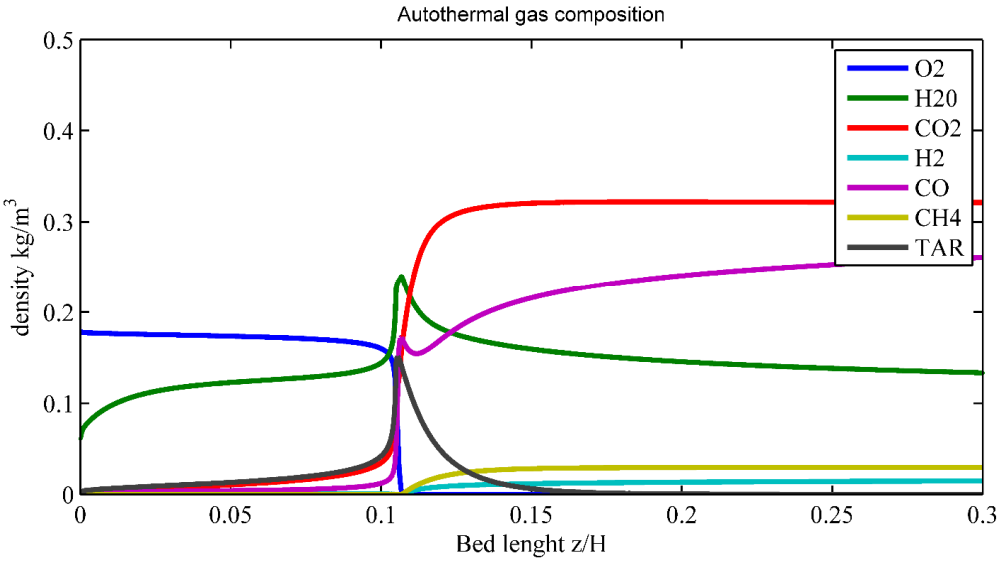

FIGURE 2: PARTIAL DENSITY OF AUTOTHERMAL GAS COMPOSITION

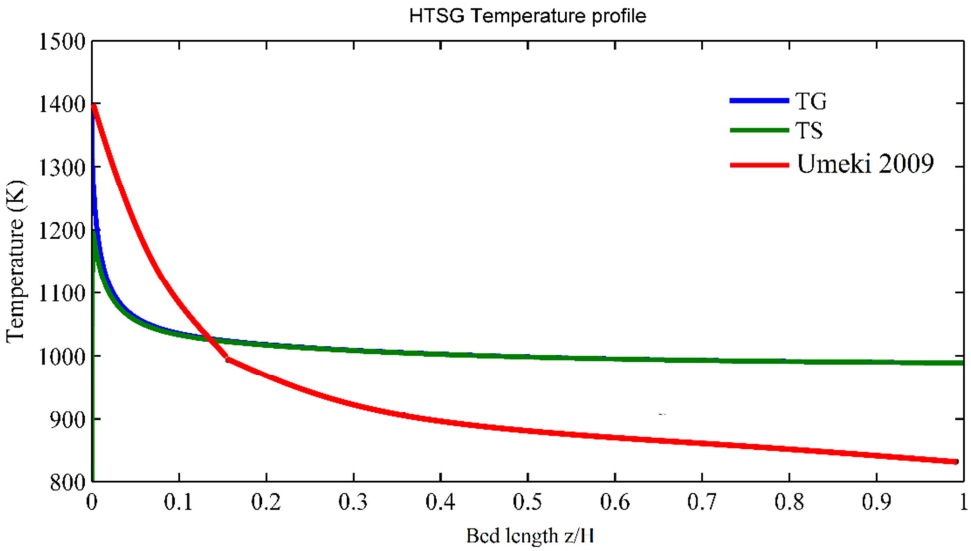

FIGURE 3: CO-CURRENT HTSG PLANT TEMPERATURE PROFILE PLOTTED AGAINST THE EXPERIMENTAL DATA OF UMEKI,2009 [11] FOR AN UPDRAFT HTSG SYSTEM, AT SAME STEAM INITIAL TEMPERATURE OF 1400K.

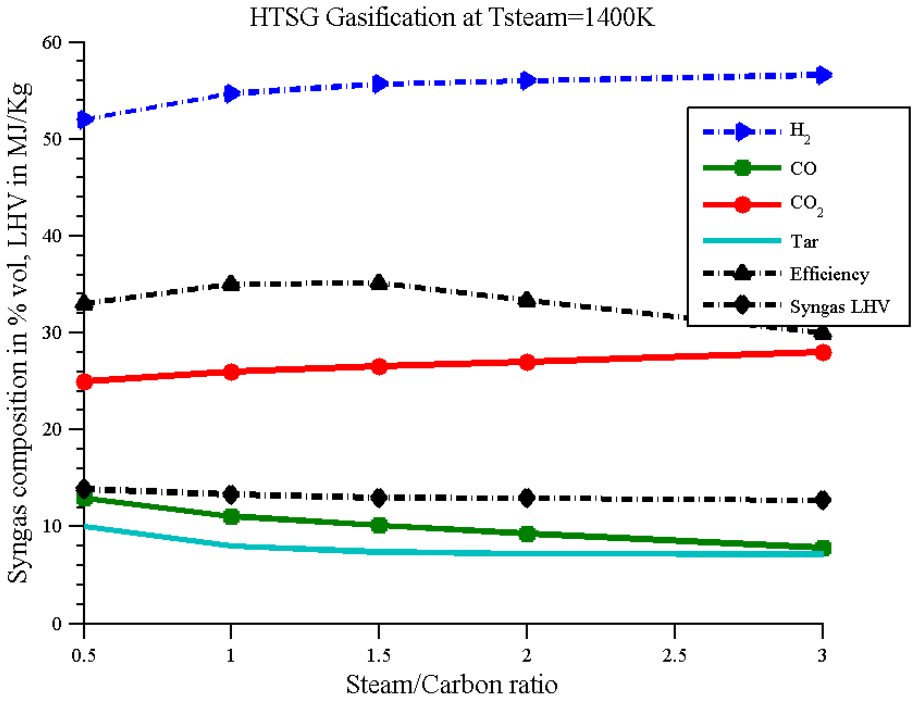

FIGURE 4: EFFECTS OF S/C RATIO ON THE HTGS GASIFICATION

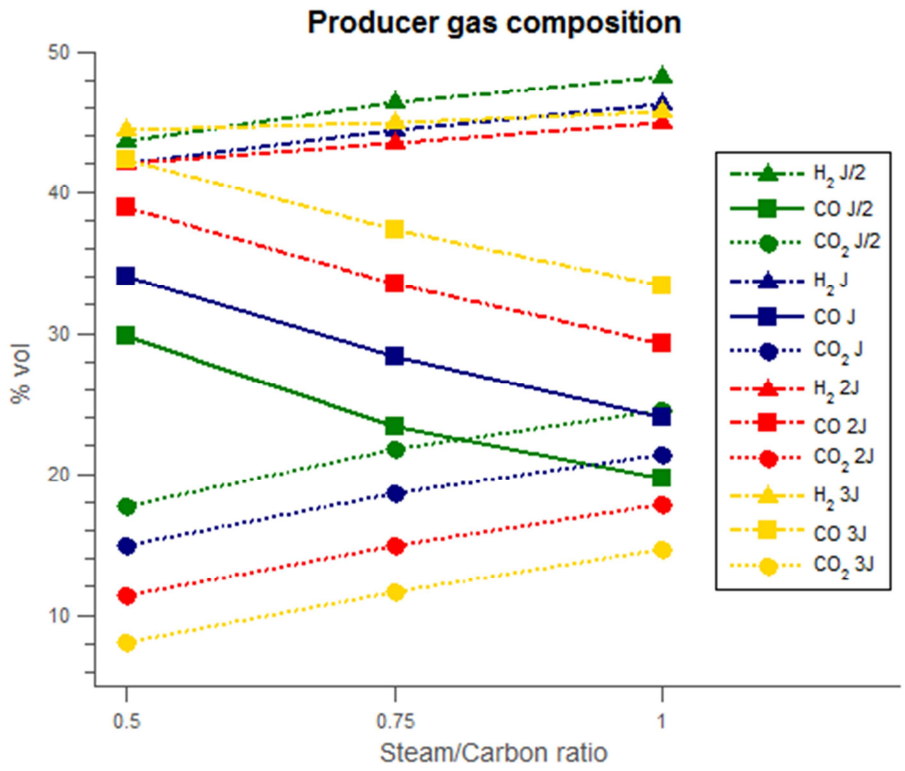

Figure 5: Influence of the S/C and flux on solar gasification

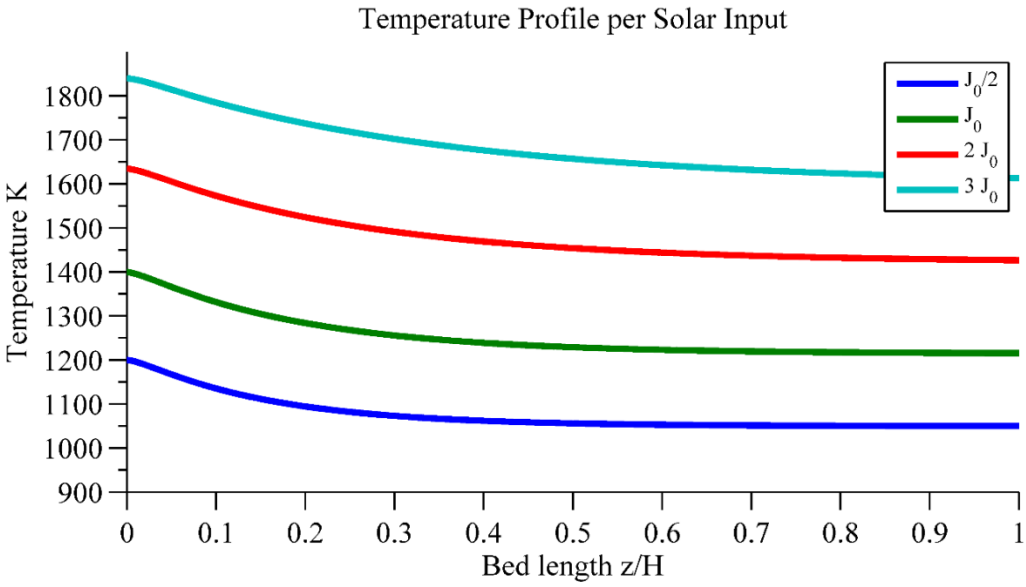

Figure 6: Showing temperature variation inside the solar reactor at different fluxes

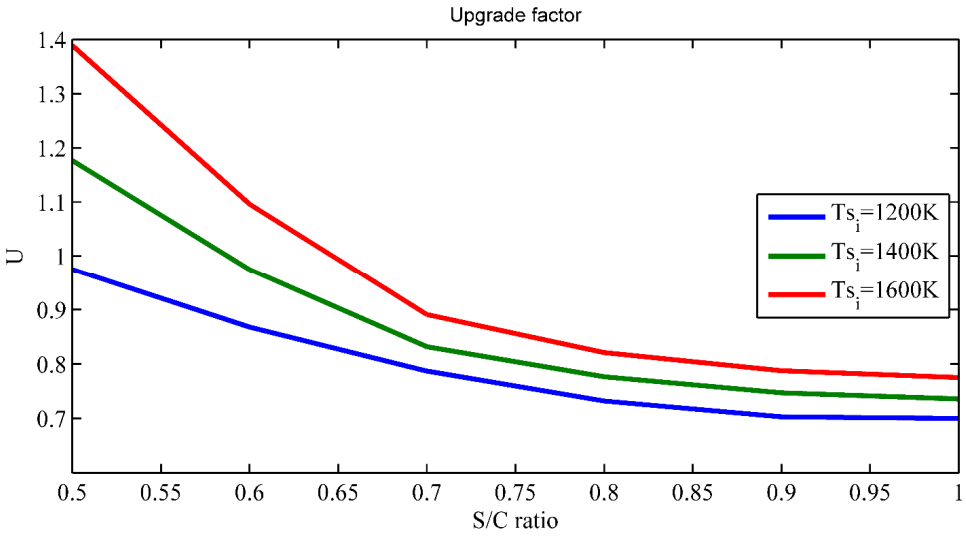

Figure 7: Solar gasification Upgrade factor dependency on solar input and steam/carbon ratio.

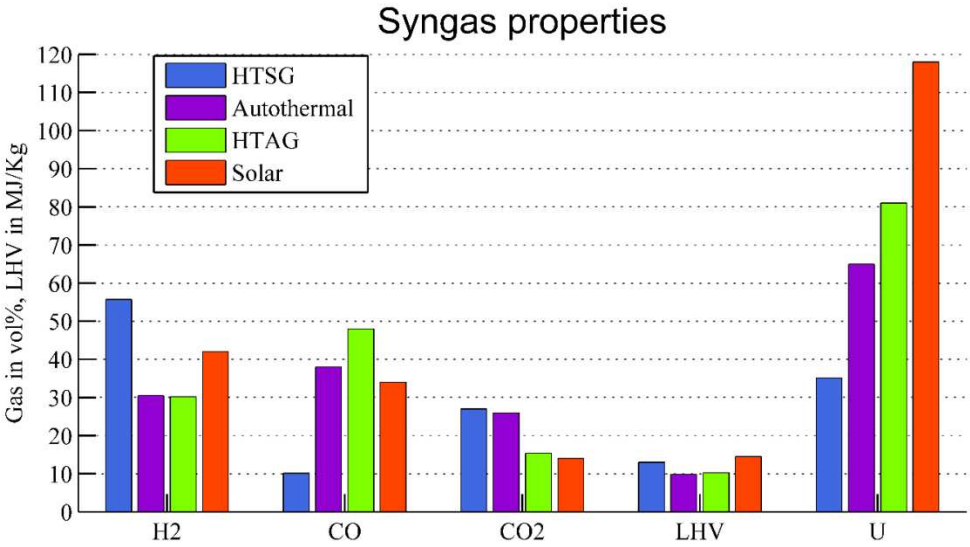

Figure 8: Performance of the different steam-gasification technologies

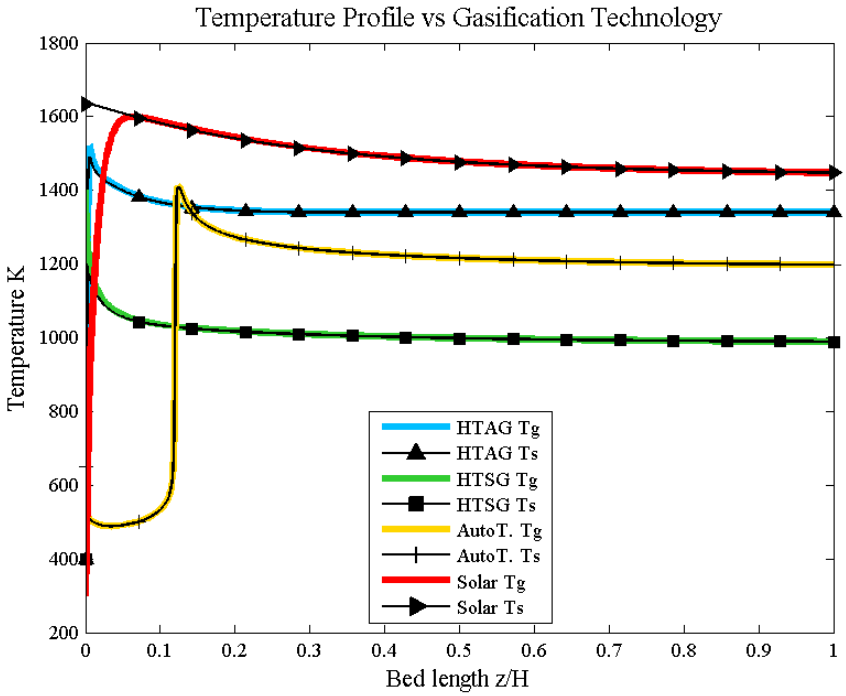

Figure 9: Comparison of the gasifier temperature for different gasification technologies